PROCEEDINGS OF SCIENCE

The evaluation of injection energy to cosmic rays from the gradient of electron temperature near the shock

Masahiro Ichihashi,[a,*] **Tomoaki Kasuga,**[a] **Hirokazu Odaka,**[a,b,c] **Aya Bamba,**[a,d,e] **Yuichi Kato,**[a] **Satoru Katsuda,**[f] **Hiromasa Suzuki**[g] **and Kazuhiro Nakazawa**[h]

[a] *Department of Physics, Graduate School of Science, The University of Tokyo, 7-3-1 Hongo, Bunkyo-ku, Tokyo 113-0033, Japan*
[b] *Kavli IPMU (WPI), UTIAS, The University of Tokyo, 5-1-5 Kashiwanoha, Kashiwa, Chiba 277-8583, Japan*
[c] *Department of Earth and Space Science, Graduate School of Science, Osaka University, 1-1 Machikaneyama-cho, Toyonaka-shi, Osaka 560-0043, Japan*
[d] *Research Center for the Early Universe, School of Science, The University of Tokyo, 7-3-1 Hongo, Bunkyo-ku, Tokyo 113-0033, Japan*
[e] *Trans-Scale Quantum Science Institute, The University of Tokyo, Tokyo 113-0033, Japan*
[f] *Graduate School of Science and Engineering, Saitama University, Shimo-Okubo 255, Sakura, Saitama 338-8570, Japan*
[g] *Department of Physics, Konan University, 8-9-1 Okamoto, Higashinada-ku, Kobe 658-8501, Japan*
[h] *Kobayashi-Maskawa Institute for the Origin of Particles and the Universe, Nagoya University, Furo-cho Chikusa, Nagoya 464-8602, Japan*

E-mail: masahiro.ichihashi@phys.s.u-tokyo.ac.jp

The injection problem is one of the biggest but unresolved issue to understand the origin of Galactic cosmic rays. To evaluate the injection energy quantitatively, we need to measure how much energy is stolen from the background thermal plasma. The injection of energy to energetic particles causes colder plasma than expected from the Rankine-Hugoniot relation in the ideal gas cases.

We measure the electron temperature gradient in the northwestern, post-shock region of SN 1006 with Chandra. It is found that the electron temperature increases from 0.52–0.62 keV at the outer edge to 0.82–0.95 keV at the inner region, 0.6 pc away from the shock front. This temperature change is lower than that expected from the Coulomb scattering, implying significant energy injection into particle acceleration in this region. For a more detailed understanding, we need observations with higher energy resolutions that will be available with XRISM and Athena.

38th International Cosmic Ray Conference (ICRC2023)
26 July - 3 August, 2023
Nagoya, Japan

*Speaker

1. Introduction

The most probable mechanism of cosmic ray acceleration is the diffusive shock acceleration. Accelerated particles emit X-rays and gamma-rays via synchrotron, inverse Compton, and pion decay (e.g. [1], [2]). Since photons are unaffected by the interstellar magnetic field, detecting them is quite important to measure the position and size of acceleration sites. Because this emission is derived from high energy particles (for example, up to 30–40 TeV in SN 1006 [3]), it is difficult to observe the initial process of cosmic ray acceleration. Because of the lack of the information of low-energy particles, we cannot know the absolute amount of the cosmic rays.

To estimate the injected energy from a shock to cosmic rays, we focus on the thermal energy of the shock-heated plasma in the downstream region. The shock wave supplies their energy to both particle acceleration and heating and bulk motion of the surrounding plasma. Most of the energy of plasma particles is thermal energy, so energy leakage to diffusive acceleration leads lower temperatures than in environments without particle acceleration.

In this study, we analyze the X-ray spectrum of the northwestern region of SN 1006, which is one of the youngest Galactic Type Ia supernova remnants (SNRs). This region has bright thermal X-ray emission [1, 4–7] and a well-measured the shock velocity. Furthermore, SN 1006 is located at 2.2 kpc [3] or ~1.5 kpc [8] from the earth. Its proximity enables us to resolve the filament structure down to ~0.005 pc with Chandra, so we can estimate the temperature structure behind the shock in detail. We divide and analyze the thermal X-ray of the northwestern region of SN 1006 and compare the estimated electron temperature to the simplest electron-heating mechanism, the Coulomb scattering model.

2. Data and Analysis

We use two data sets of the northwestern region of SN 1006 with the longest exposures: ObsID 1959 (observed in 2001) and ObsID 13737 (observed in 2012) (see Figure 1). These data are reprocessed and analyzed with the software packages Chandra Interactive Analysis of Observation (CIAO) version 4.13.0 [9], CALDB 4.9.4 and XSPEC software version 12.11.1 [10]. The resultant exposure is 88.98 ks (ObsID 1959) and 87.09 ks (ObsID 13737), respectively. We use the C-statistic [11] for our analysis below.

In this study, we consider the background by using the background model with two types of components, the particle induced background (PIB) and the sky background. PIB is the background induced by cosmic-ray particles, which depends on both the solar activity and the property of the detector, and the sky background is the emission from celestial sources. In this analysis, PIB is modeled by using `mkacispback` package [12]. The sky background is modeled following Uchida et al. [6] and fitted the spectrum of the blank sky of ObsID 13737. The sky background of Uchida et al. [6] has four components, but some of them are not contributed to the blank sky of our data. The components we finally use are a power law component due to local excess and an ionization equilibrium collisional plasma model due to Lupus Loop.

In the analysis of the spectrum, we divide the northwestern region of SN 1006 into twelve regions (see Figure 1). Each of them has a rectangular shape of $140'' \times 15''$ or 1.5 pc $\times$ 0.16 pc at 2.2 kpc distance. The long side of three regions nearest to the shock front coincides with the

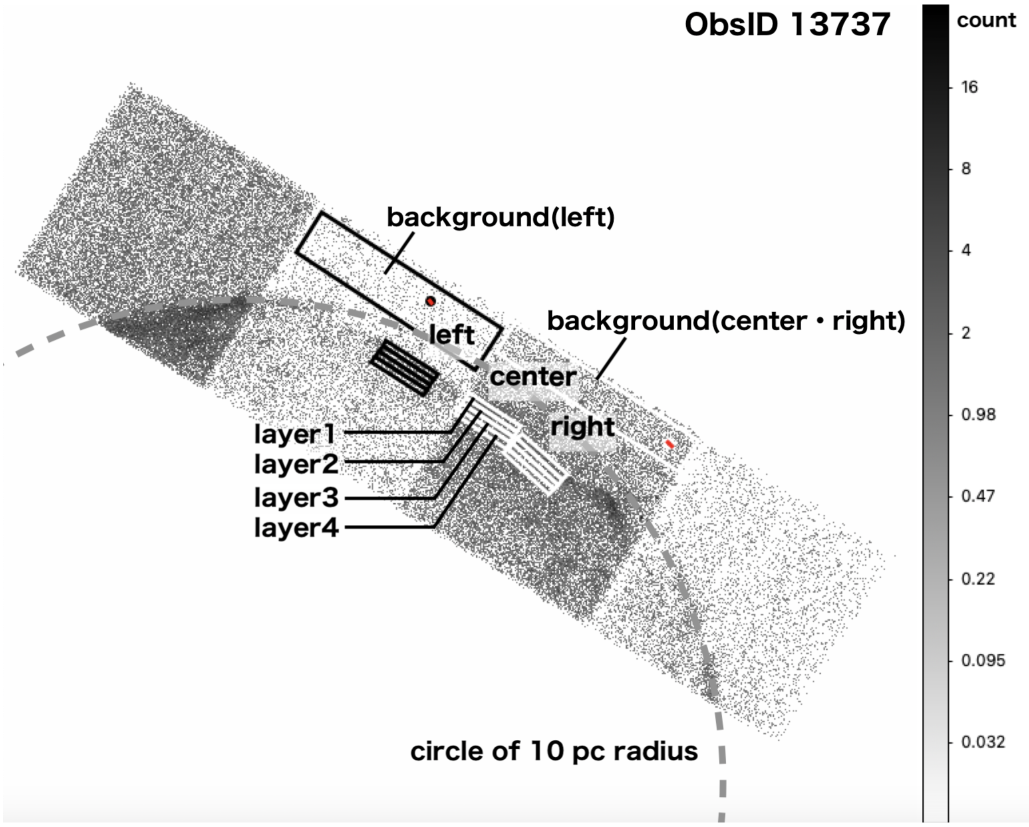

Figure 1: The 0.5–2.0 keV image of the northwestern region of SN 1006 observed by *Chandra* (ObsID : 13737). The image is shown on a log scale. For each of the left, center, and right regions, the four layers from the filament toward downstream are labeled as layer 1, 2, 3, and 4 as described for the center regions. Gray dashed circle is a circle of 10 pc radius which approximating the shock front in SN 1006 without the northwestern region, The northwestern region collides to $\mathrm{H_I}$ region, and has 86 arcsec = 0.93 pc indentation.

shock front of each observation, and the long side of two regions located side-by-side coincides with each other. They are labeled as shown in Figure 1. Figure 2 shows the comparison of the spectrum from layer 1 (on the shock front) and 4 (innermost) in the center region. One can see that the spectrum from layer 1 shows softer spectrum compared with that from layer 4. This implies that the electron temperature is higher in the inner regions than the outermost regions. To evaluate the change of electron temperature quantitatively, we fit all extracted spectra by using an absorbed non-equilibrium ionization collisional plasma model with variable abundance (VNEI) [13]. We assume that the emission is from the shocked interstellar medium heated by the shockwave, since the region we observed is very close to the shock front and not contaminated severely by the ejecta from its progenitor [6]. Also, we do not consider the non-thermal X-ray components from electrons accelerated on the shock front ([1], [14]), because the X-ray emission from this part of SN 1006 is mostly from the shock-heated plasma (e.g., [7]). The interstellar absorption is considered by the `phabs` model, for which the hydrogen column density is fixed to $N_{\mathrm{H}} = 4.16 \times 10^{20}$ cm^{-2} ([15]) with solar abundance [16].

The fitting result is acceptable with the c-statistics/d.o.f. (degree of freedom) of 16012.98/15564. Note that the sky background level has some uncertainties. We perform the same analysis with the

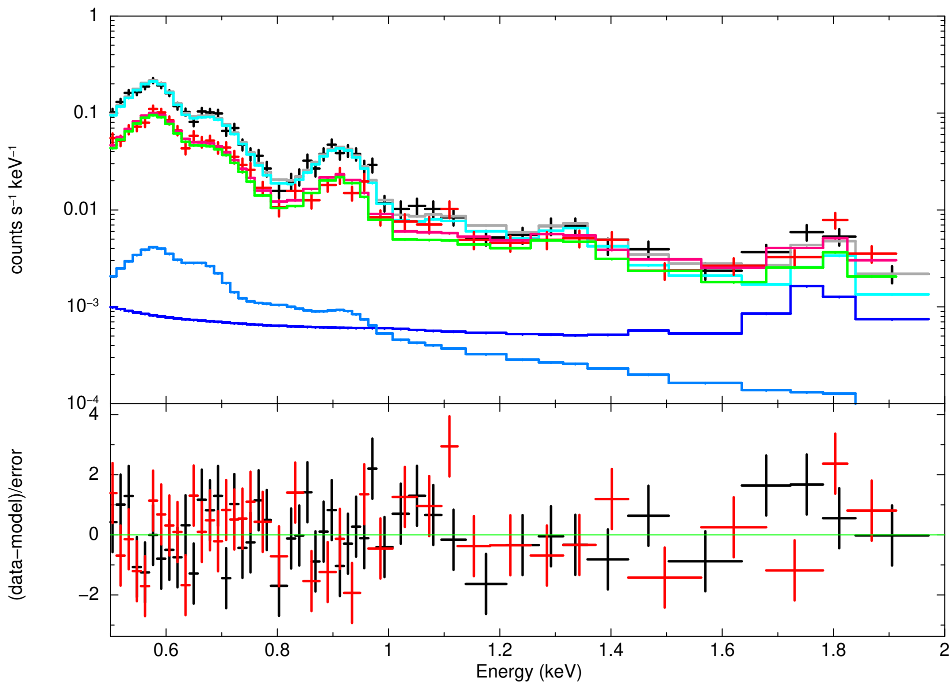

Figure 2: Comparison of spectra of center region of ObsID 13737. Black and red data show the spectrum from layer 1 and layer 4, respectively. Other lines in the upper panel shows the components of the best-fit model: gray and magenta line shows the sum of all components of the best-fit model of layer 1 and layer 4, green and light blue line show the source component of layer 1 and layer 4, cyan line shows the sky background and blue line show the PIB component.

background normalization increased or decreased within their error range compared to the best-fit value and find no significant difference in our results. Figure 3 shows the variation of the electron temperature in each of the left, center and right region. One can see that the temperature gradually increases from the layer 1 to 4.

3. Discussion

We compare our finding of the increase of the electron temperature to the simplest electron heating process, the Coulomb scattering model.

The Coulomb scattering can be scaled by a product of electron density (n_e) and the time after the shock heating, i.e., the plasma age (t). The electron density can be estimated from the emission measure by assuming the volume of the observation region. The shockwave of the northwestern region of SN 1006 collides with the H_I region, so the shape of the northwestern region of SN 1006 has a $\sim$ 0.93 pc indentation from a sphere with a radius of 10 pc. Considering this indentation from a sphere, we calculate the volume and the electron density of the observation regions. The plasma age can be estimated from the distance from the shock front and the shock speed. The shock speeds depend on regions in SN 1006: 2800 km s^{-1} in the northwestern region [17] and $\sim$ 6000 km s^{-1} in other regions [18]. This difference implies that the shock speed decreased by a collision to the H_I region. Considering a $\sim$ 0.93 pc indentation, we estimate that the collision between SN 1006 and

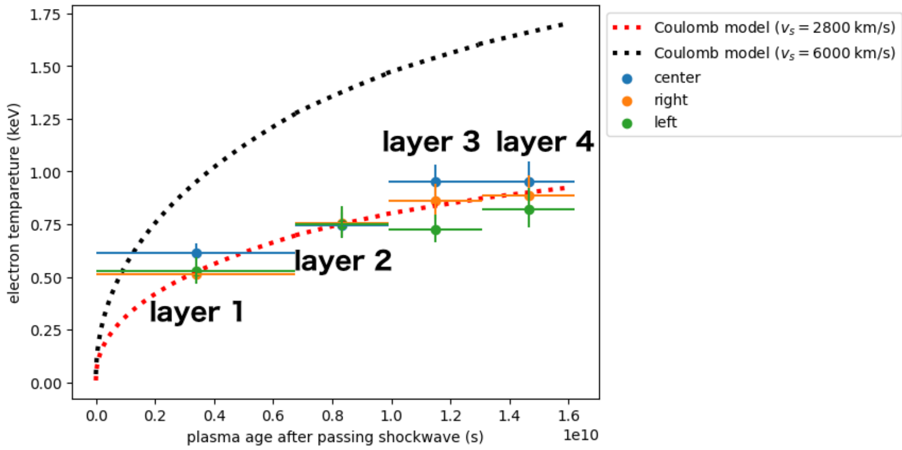

Figure 3: Comparison of the observed electron temperatures with those estimated from the Coulomb scattering model. The shock speed is assumed as 2800 km s^{-1} at the red line and 6000 km s^{-1} at the black line. The initial temperature is assumed as the temperature estimated from the Rankin-Hugoniot relation.

$\mathrm{H_I}$ region occurred about 250 years ago, which corresponds to the plasma age of the boundary of our observation regions between layer 1 and layer 2. Based on this estimation, we assume in this comparison the speeds of the shock passing through the layer 1 and layers 2–4 to be 2800 km s^{-1} and 6000 km s^{-1}, respectively.

The result of the comparison between our observation and the Coulomb scattering model is shown in Figure 3. In the layer 1, the observation is consistent with the Coulomb scattering model where the shock speed is 2800 km s^{-1} and β $(= T_e/T_p) \leq 0.03$. This result does not contradict the estimation that the shock speed is 2800 km s^{-1} in the layer 1. On the other hand, the electron temperatures in layers 2, 3 and 4, where the shock wave passes through before the collision and the shock speed is assumed to be 6000 km s^{-1}, are significantly lower than that estimated from the Coulomb scattering model.

One of the possible reasons of this discrepancy between our observed electron temperatures in layers 2, 3 and 4 and the Coulomb scattering model is an energy leakage to the cosmic ray acceleration: the efficient injection of the energy from the shock to the particle acceleration. On the other hand, we should be careful about projection effects. Given the temperature gradient in the post shock region as we measured, it is natural to see apparently cooler plasmas in the inner region unless we consider the projection effect in our spectral analysis. Because of the lack of the statistics, we cannot quantify the projection effect in this study. We expect improved statistics with good spatially resolving power in the future work.

Ion temperatures can be measured using the Doppler broadening of characteristic X-ray lines from the plasma. In order to measure the ion temperature precisely, our observations lack the energy resolution. For precise measurements of the widths of their characteristic X-ray lines, we need future satellites with higher energy resolutions, such as XRISM [19] or Athena [20]. In particular, XRISM is going to be launched and start operations soon. We expect XRISM observations to find the decrease of ion temperatures and evaluate the amount of accelerated cosmic rays behind the shock wave of SNRs.

4. Conclusion

We analyze the northwestern region of SN 1006 with Chandra and measure the spatial variation of the electron temperature just behind the shock. The electron temperature increases toward downstream. The temperature gradient is significantly lower than that expected from the Coulomb scattering model. One of the possible reasons of this discrepancy is the energy leakage to the cosmic ray acceleration, but we have not yet obtained definitive proof of this hypothesis. We will measure the ion temperature near the shock front by using future satellites such as XRISM and Athena and will evaluate the amount of energy leakage to the cosmic ray acceleration.

References

[1] Koyama, K., Petre, R., Gotthelf, E. V., et al. 1995, Nature, 378, 255. doi:10.1038/378255a0

[2] Aharonian, F. A., Akhperjanian, A. G., Aye, K.-M., et al. 2004, Nature, 432, 75. doi:10.1038/nature02960

[3] Winkler, P. F., Gupta, G., & Long, K. S. 2003, ApJ, 585, 324. doi:10.1086/345985

[4] Bamba, A., Fukazawa, Y., Hiraga, J. S., et al. 2008, PASJ, 60, S153. doi:10.1093/pasj/60.sp1.S153

[5] Winkler, P. F., Williams, B. J., Blair, W. P., et al. 2013, ApJ, 764, 156. doi:10.1088/0004-637X/764/2/156

[6] Uchida, H., Yamaguchi, H., & Koyama, K. 2013, ApJ, 771, 56. doi:10.1088/0004-637X/771/1/56

[7] Li, J.-T., Decourchelle, A., Miceli, M., et al. 2016, MNRAS, 462, 158. doi:10.1093/mnras/stw1640

[8] Katsuda, S. 2017, Handbook of Supernovae, 63. doi:10.1007/978-3-319-21846-5_45

[9] Fruscione, A., McDowell, J. C., Allen, G. E., et al. 2006, Proc.SPIE, 6270, 62701V. doi:10.1117/12.671760

[10] Arnaud, K. A. 1996, Astronomical Data Analysis Software and Systems V, 101, 17

[11] Cash, W. 1979, ApJ, 228, 939. doi:10.1086/156922

[12] Suzuki, H., Plucinsky, P. P., Gaetz, T. J., et al. 2021, AAP, 655, A116. doi:10.1051/0004-6361/202141458

[13] Keith Arnaud, Craig Gordon, Ben Dorman & Kristin Rutkowski, Xspec Users' Guide for version 12.13, NASA, 2022, https://heasarc.gsfc.nasa.gov/xanadu/xspec/manual/node195.html, (referred on 2023-07-03)

[14] Bamba, A., Yamazaki, R., Ueno, M., et al. 2003, ApJ, 589, 827. doi:10.1086/374687

PoS(ICRC2023)387

[15] Broersen, S., Vink, J., Miceli, M., et al. 2013, AAP, 552, A9. doi:10.1051/0004-6361/201220526

[16] Anders, E. & Grevesse, N. 1989, Acta, 53, 197. doi:10.1016/0016-7037(89)90286-X

[17] Katsuda, S., Long, K. S., Petre, R., et al. 2013, ApJ, 763, 85. doi:10.1088/0004-637X/763/2/85

[18] Winkler, P. F., Williams, B. J., Reynolds, S. P., et al. 2014, ApJ, 781, 65. doi:10.1088/0004-637X/781/2/65

[19] Tashiro, M., Maejima, H., Toda, K., et al. 2020, Proc. SPIE, 11444, 1144422. doi:10.1117/12.2565812

[20] Nandra, K., Barret, D., Barcons, X., et al. 2013, arXiv:1306.2307. doi:10.48550/arXiv.1306.2307